blood®
Plenary Paper

PHAGOCYTES, GRANULOCYTES, AND MYELOPOIESIS

Macrophage NOX2 NADPH oxidase maintains alveolar homeostasis in mice

Sourav Bhattacharya,[1] Rachel A. Idol,[1] Wei Yang,[2] Jorge David Rojas Márquez,[3] Yanan Li,[1] Guangming Huang,[1] Wandy L. Beatty,[4] Jeffrey J. Atkinson,[5] John H. Brumell,[3,6-8] Juhi Bagaitkar,[9-11] Jeffrey A. Magee,[1] and Mary C. Dinauer[1,12]

[1]Department of Pediatrics and [2]Department of Genetics, Washington University School of Medicine in St. Louis, St. Louis, MO; [3]Cell Biology Program, Hospital for Sick Children, Toronto, ON, Canada; [4]Department of Molecular Microbiology and [5]Department of Medicine, Washington University School of Medicine in St. Louis, St. Louis, MO; [6]Institute of Medical Science and [7]Department of Molecular Genetics, University of Toronto, Toronto, ON, Canada; [8]Sick Kids Inflammatory Bowel Disease Centre, Hospital for Sick Children, Toronto, ON, Canada; [9]Department of Oral Immunology and Infectious Diseases, University of Louisville, Louisville, KY; [10]Abigail Wexner Research Institute at Nationwide Children's Hospital and [11]Department of Pediatrics, The Ohio State University College of Medicine, Columbus, OH; and [12]Department of Pathology and Immunology, Washington University School of Medicine in St. Louis, St. Louis, MO

KEY POINTS

- **Mice with inactivation of NOX2, globally or in macrophages, spontaneously acquire an activated alveolar macrophage phenotype by adulthood.**
- **Epigenetic and transcriptional profiles of NOX2-deleted AMs are influence by their niche and primed to generate inflammation.**

The leukocyte NADPH oxidase 2 (NOX2) plays a key role in pathogen killing and immunoregulation. Genetic defects in NOX2 result in chronic granulomatous disease (CGD), associated with microbial infections and inflammatory disorders, often involving the lung. Alveolar macrophages (AMs) are the predominant immune cell in the airways at steady state, and limiting their activation is important, given the constant exposure to inhaled materials, yet the importance of NOX2 in this process is not well understood. In this study, we showed a previously undescribed role for NOX2 in maintaining lung homeostasis by suppressing AM activation, in CGD mice or mice with selective loss of NOX2 preferentially in macrophages. AMs lacking NOX2 had increased cytokine responses to Toll-like receptor-2 (TLR2) and TLR4 stimulation ex vivo. Moreover, between 4 and 12 week of age, mice with global NOX2 deletion developed an activated CD11b^{high} subset of AMs with epigenetic and transcriptional profiles reflecting immune activation compared with WT AMs. The presence of CD11b^{high} AMs in CGD mice correlated with an increased number of alveolar neutrophils and proinflammatory cytokines at steady state and increased lung inflammation after insults. Moreover, deletion of NOX2 preferentially in macrophages was sufficient for mice to develop an activated CD11b^{high} AM subset and accompanying proinflammatory sequelae. In addition, we showed that the altered resident macrophage transcriptional profile in the absence of NOX2 is tissue specific, as those changes were not seen in resident peritoneal macrophages. Thus, these data demonstrate that the absence of NOX2 in alveolar macrophages leads to their proinflammatory remodeling and dysregulates alveolar homeostasis.

Introduction

The phagocyte NADPH oxidase 2 (NOX2) generates superoxide, the precursor to reactive oxygen species (ROS) that play essential roles in host defense and immunoregulation.[1] Inherited defects in the NOX2 enzyme complex lead to chronic granulomatous disease (CGD), characterized by recurrent, severe bacterial and fungal infections, and aberrant inflammation.[2] CGD results from inactivating recessive mutations in any of several genes for different subunits of NOX2, including X-linked *CYBB*, which encodes a membrane flavocytochrome, and autosomal genes for *CYBBA*, *NCF1*, *NCF2*, or *NCF4*, which encode critical regulatory subunits, or *CYBC1*, an endoplasmic reticulum protein important for CYBB biosynthesis.[2] Manifestations of CGD typically involve barrier sites, frequently the lung.[1,3,4] Indeed, a chronic lung disease afflicts many young adult patients with CGD and is not always a sequela of prior pneumonias but may instead reflect a noninfectious inflammatory response.[3-8] Sterile lung inflammation is also reported in CGD mice.[9,10] These observations raise the question of whether NOX2 modulates immune responses within the lungs to maintain homeostasis under basal conditions.

In the lung, residential alveolar macrophages (AMs), which are long lived, self-renewing cells derived from fetal monocyte precursors, constitute ≈95% of immune cells in the airways at steady state.[11,12] Tissue macrophages are essential as both a first line of host defense and for conducting tissue-specific functions under homeostatic and inflammatory conditions.[13-16] Their ability to adapt to specific tissue niches and maintain homeostasis is governed by signals in the local microenvironment as well as cell-intrinsic epigenetic and transcriptional remodeling.[16-22]

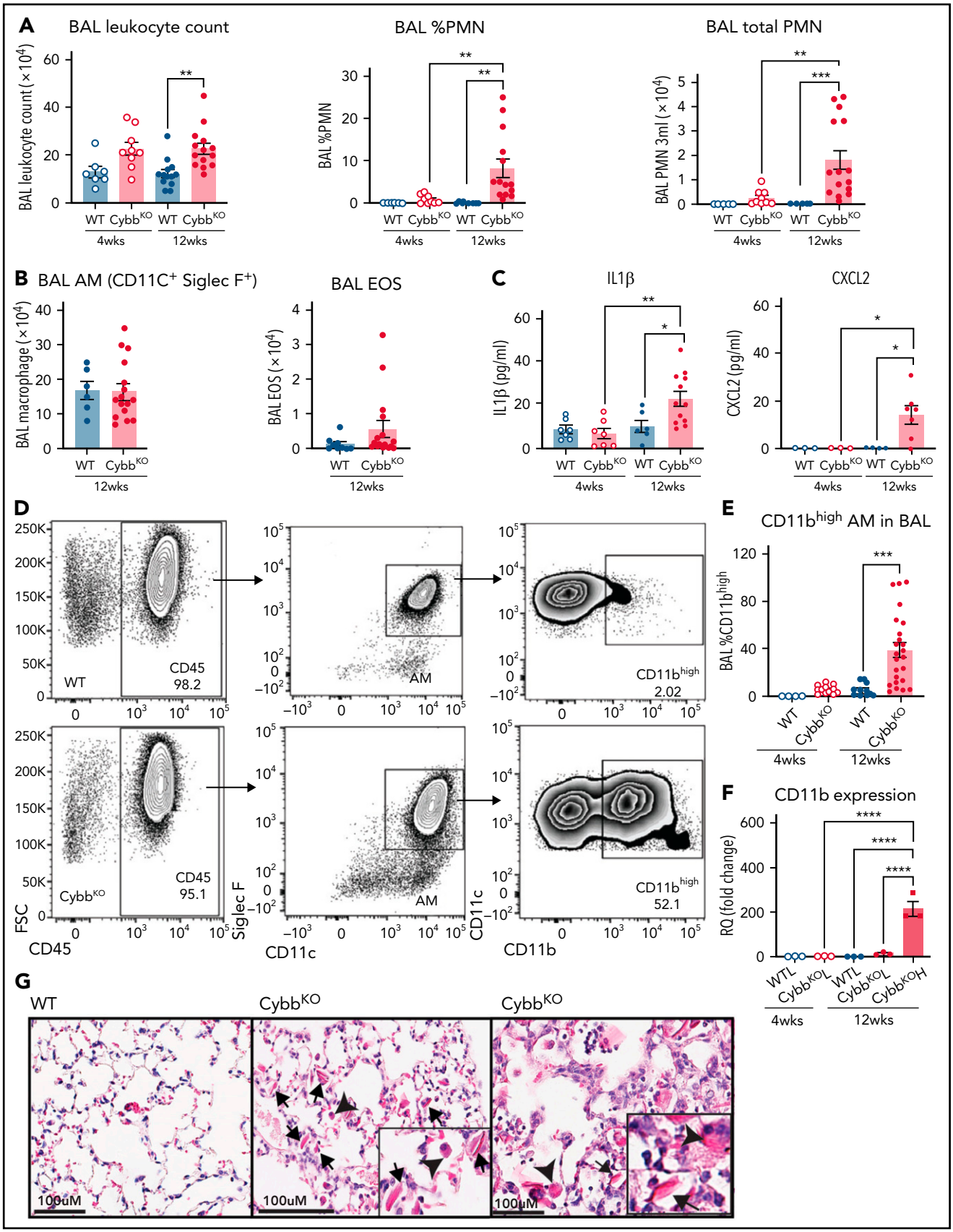

Figure 1.

AMs are strategically located on the luminal side of the alveoli, where they continually sample the environment and respond accordingly.[11,23,24] To limit collateral tissue damage, AMs maintain a relatively high threshold for inflammatory activation by inhaled materials, unless potentially infectious.[11,24] Molecular mechanisms that prevent de novo polarization in hyperreactive states are incompletely understood.

We investigated the cell-intrinsic role of NOX2 in AMs, as studied in mice with either global or cell type–restricted deletion of NOX2. NOX2-deficient mice spontaneously developed AMs that were epigenetically, transcriptionally, and phenotypically distinct from wild-type (WT) AMs, including a proinflammatory CD11b^{high} AM population. These changes became evident as the mice reached adulthood, coinciding with increased alveolar neutrophils and inflammatory mediators, independent of host or environmental microbes. Moreover, NOX2-deleted AMs exhibited heightened activation ex vivo, and mice with either global or macrophage deletion of NOX2 displayed enhanced lung inflammation after insults. Thus, NOX2 is essential for modulating AM responses that maintain pulmonary homeostasis.

Methods

Details of experimental procedures are provided in the supplemental Methods (available on the *Blood* Web site).

Mice

Experiments were conducted in accordance with the *Guide for the Care and Use of Laboratory Animals*, under protocols approved by the Institutional Animal Care and Use Committee at Washington University in St. Louis, and the Animal Care Committee of the University of Louisville or the Hospital for Sick Children. WT C57BL/6J mice were purchased from The Jackson Laboratory or were bred in-house. X-linked CGD[25] (*Cybb*^{KO}), *Ncf2*$^{-/-}$[26] (*Ncf2*^{KO}), *Ncf2*$^{fl/fl}$, and *Ncf2*$^{fl/fl}$ LysM$^{WT/Cre}$ (*Ncf2*$^{LysM\text{-}Cre}$) mice were bred in-house. *Cybb*^{KO} *Ifnar1*^{KO} mice[27] were bred in the Animal Care Facility of the Hospital for Sick Children. The mice were maintained under specific-pathogen–free conditions, which included monitoring for pathogenic bacteria and viruses, or, for germ-free *Cybb*^{KO} mice, under gnotobiotic conditions at the University of Louisville Gnotobiotic Mouse Facility. Both male and female mice were studied at the indicated ages.

In vivo studies

Bronchoalveolar lavage (BAL), lung cell suspensions, and lung histology were analyzed[28] in naive mice. The mice were also challenged with intranasal zymosan (1 μg/g), and lung inflammation was analyzed after 18 hours.[28] In other studies, the mice were challenged with intraperitoneal zymosan (0.05 mg/g) and peritoneal, and lung inflammation was analyzed after 48 hours.[28-31]

Macrophage stimulation ex vivo

AMs and resident peritoneal macrophages (RPMs) isolated from naïve mice were plated in 96-well tissue culture plates. After adhesion, cells were treated with UltraPure lipopolysaccharide (LPS; *Escherichia coli*, 10 ng/mL; Invivogen,) or Pam3csk4 (100 ng/mL; Invivogen) for 4 hours at 37°C. Gene expression was studied by quantitative reverse transcription-polymerase chain reaction (qRT-PCR).

Macrophage sorting for transcriptional and epigenetic analysis

RNA sequencing (RNA-seq) and assay for transposase accessible chromatin sequencing (ATAC-seq) were performed on BAL AMs (CD45$^+$Ly6G$^-$CD11c$^+$Sigle F$^+$) sorted on the basis of CD11b expression. RNA microarray analysis was performed on RPMs sorted as B220$^-$CD115$^+$F4/80^{high}MHC class II$^-$ and B220$^-$F4/80^{low}MHC class II^{high}.

Statistics

Unpaired Student *t* tests were used to compare 2 groups, and 1-way analysis of variance, followed by Tukey's post hoc test, was used to compare among multiple groups. For nonparametric data, unpaired, 2-tailed Mann-Whitney tests were used. Data were analyzed and graphed with Prism 5 (GraphPad Software, Inc).

Results

Mice with global deletion of NOX2 spontaneously develop lung inflammation and a population of CD11b^{high} AMs

To investigate mechanisms underlying the spontaneous development of lung inflammation in CGD mice in the absence of infection, we used CGD mice with inactivating mutations in *Cybb* (*Cybb*^{KO} mice[25]) or *Ncf2* (*Ncf2*^{KO} mice[26]) and also developed mice with LysM-Cre–mediated deletion of *Ncf2* (*Ncf2*^{LysMCre} mice).

As a starting point, we examined the inflammatory status of the lungs at 4 and 12 weeks of age in WT and *Cybb*^{KO} mice. BAL samples from 4-week-old WT and *Cybb*^{KO} mice had similar total leukocyte counts with few neutrophils (Figure 1A). However, these were significantly increased in 12-week-old *Cybb*^{KO} mice (Figure 1A). The number of BAL AMs and eosinophils was similar in both genotypes (Figure 1B). *Ncf2*^{KO} CGD mice showed comparable findings (data not shown). Multiplex analysis of BAL from 12-week-old *Cybb*^{KO} mice showed significantly higher levels of tumor

Figure 1. Mice with global deletion of NOX2 develop lung inflammation and a subset of CD11b^{high} AMs. (A) BAL leukocyte count, flow cytometric analysis of the percentage of polymorphonuclear leukocytes (PMNs) and total PMNs in 3 mL BAL from 4- and 12-week-old WT and *Cybb*^{KO} male and female mice (n ≥ 7 in each group). (B) Flow cytometric analysis of total AMs (CD45$^+$Siglec F$^+$CD11c$^+$ cells) and total eosinophils (EOS) (CD45$^+$Siglec F$^+$CD11c$^-$ cells) from 3 mL of BAL (n ≥ 7). (C) ELISA of IL-1β and CXCL2 in BAL (n ≥ 3 in each group). (D) Gating strategy to identify CD11b$^+$ AMs in the BAL (CD45$^+$SIglec F$^+$ CD11c$^+$CD11b^{high}). (E) Percentage of AMs that are CD11b^{high} in BAL samples from different groups (n ≥ 4). (F) CD11b expression by qRT-PCR in flow-sorted AMs of different groups. WTL, WT CD11b^{low} AMs; *Cybb*^{KO} L, *Cybb*^{KO} CD11b^{low} AMs; and *Cybb*^{KO} H, *Cybb*^{KO} CD11b^{high} AMs (n = 3). (G) Lung sections from 12-week-old WT and *Cybb*^{KO} mice, as indicated, stained with hematoxylin-eosin showing intracellular (arrowhead) and extracellular eosinophilic crystals (arrow) in *Cybb*^{KO} mice. The rightmost panel shows lung tissue from a *Cybb*^{KO} mouse with small infiltrates adjacent to some of the crystals. Scale bars, 100 μm. Representative images from ≥5 mice of each genotype. Bar graph data are expressed as mean ± standard error of the mean. The Student *t* test was performed for samples distributed in 2 groups. *P < .05; **P < .01; ***P < .001. One-way analysis of variance was performed followed by Tukey's post hoc analysis comparing multiple groups. Data represent at least 2 independent experiments. *P < .05; **P < .01; ***P < .001; ****P < .0001. ELISA, enzyme linked immunosorbent assay.

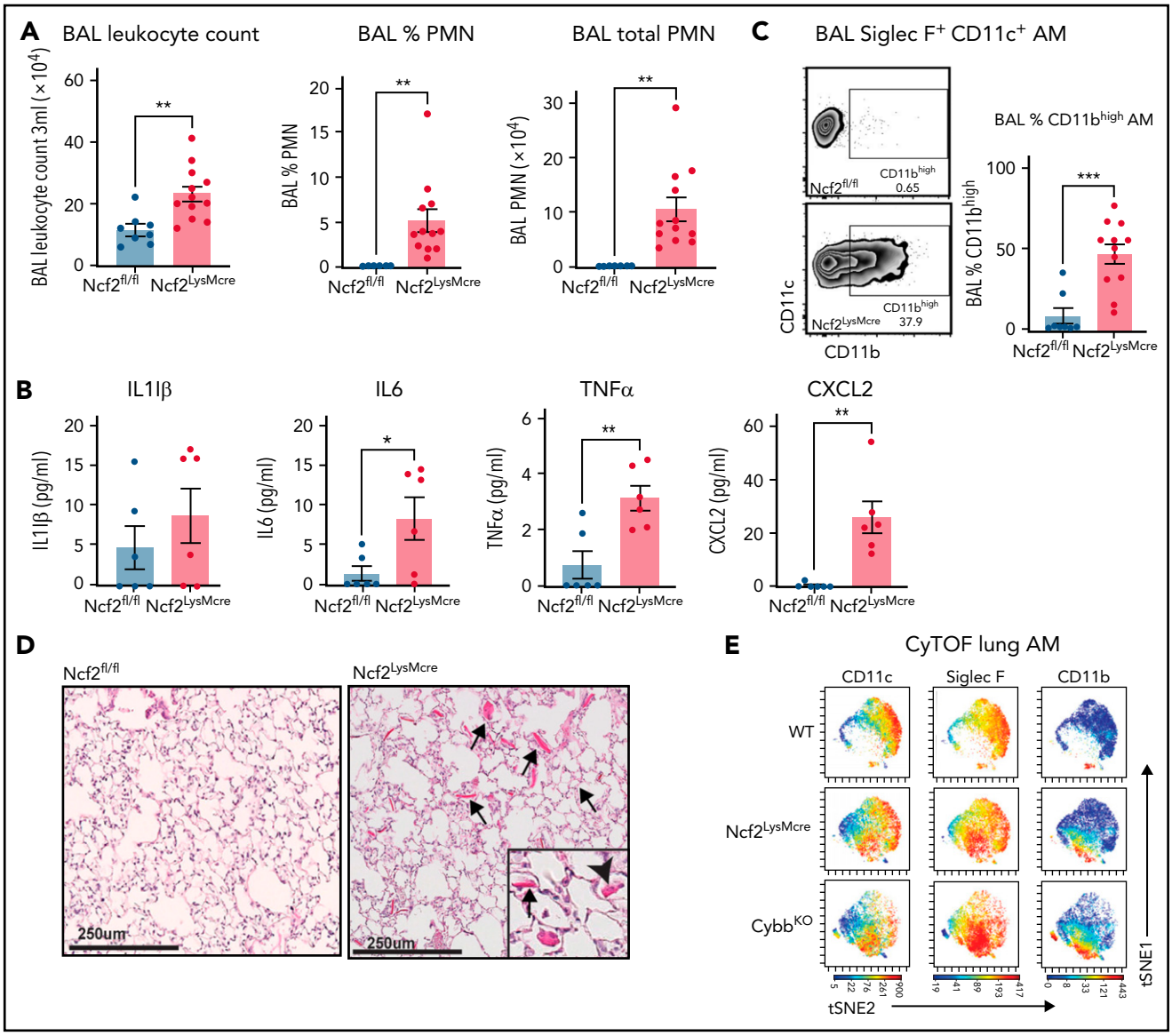

Figure 2. Mice with *LysM*Cre-mediated deletion of NOX2 exhibit an inflammatory lung phenotype. (A) BAL leukocyte count, flow-cytometric analysis of the percentage of polymorphonuclear leukocytes (PMNs), and total PMNs in 3 mL BAL from 12-week-old *Ncf2*$^{fl/fl}$ and *Ncf2*^{LysMCre} mice (n ≥ 7). (B) ELISA analysis of BAL samples from 12-week-old mice (n ≥ 6). (C) Flow cytometric analysis of CD11c^{+}CD11b^{high} macrophages from the CD45^{+}Siglec F^{+} CD11c^{+} gate and the percentage that are CD11b^{high} in BAL samples of 12-week-old mice (n ≥ 8). (D) Lung sections from12-week-old *Ncf2*$^{fl/fl}$ and *Ncf2*^{LysMcre} mice stained with hematoxylin-eosin showing intracellular (arrowhead) and extracellular (arrow) eosinophilic crystals. Bars represent 250 μm. Representative images from more than 6 samples per genotype. (E) tSNE plot from CyTOF data of CD45^{+}CD11c^{+}Siglec F^{+} AMs from lung tissue harvested from 12-week-old WT, *Cybb*^{KO} and *Ncf2*^{LysMcre} mice showing populations expressing CD11c, Siglec F, and CD11b. Representative plots from ≥4 samples in each group. Bar graph data are expressed as the mean ± standard error of the mean. The Student *t* test was performed for samples distributed in 2 groups. Data represented the results of at least 2 independent experiments. *$P < .05$; **$P < .01$; ***$P < .001$. CyTOF, cytometry by time of flight; t-SNE, *t*-distributed stochastic neighbor embedding.

necrosis factor-α (TNF-α), interferon-α (IFN-α), interleukin-1β (IL-1β), IL-18, and chemokines, along with reduced IL-10 than the WT BAL analysis (supplemental Figure 2A). BAL IL-1β and CXCL2 levels measured by enzyme-linked immunosorbent assay were similar in 4-week-old WT and *Cybb*^{KO} mice, but were increased in 12-week-old *Cybb*^{KO} mice (Figure 1C). Together, these results set a timeline for the spontaneous development of an inflammatory alveolar state in CGD mice from 4 to 12 weeks after birth.

Next, we examined AM surface markers by flow cytometry to evaluate whether they changed as lungs became inflamed in *Cybb*^{KO} mice. Although AMs with a conventional marker phenotype (CD45^{+}CD11c^{high}Siglec F^{high}CD11b^{low32}) were present, we identified an additional CD11c^{high}Siglec F^{high}CD11b^{high} population in BAL and lung tissue of 12-week-old *Cybb*^{KO} mice, representing ∼40% of the total AMs (Figure 1D-E; supplemental Figure 1A-B). This CD11b^{high} subset, which had increased CD11b transcription (Figure 1F), was virtually absent in 4-week-old *Cybb*^{KO} and WT mice (Figure 1E). At homeostasis, AMs both self-renew in situ and are slowly replaced in adulthood by bone marrow–derived precursors.[33] CD11c^{high}Siglec F^{high}CD11b^{high} "activated" macrophages in the BAL, which were derived from resident AMs, have been identified in various inflammatory settings, monocytes, or both.[34-36] Expression of

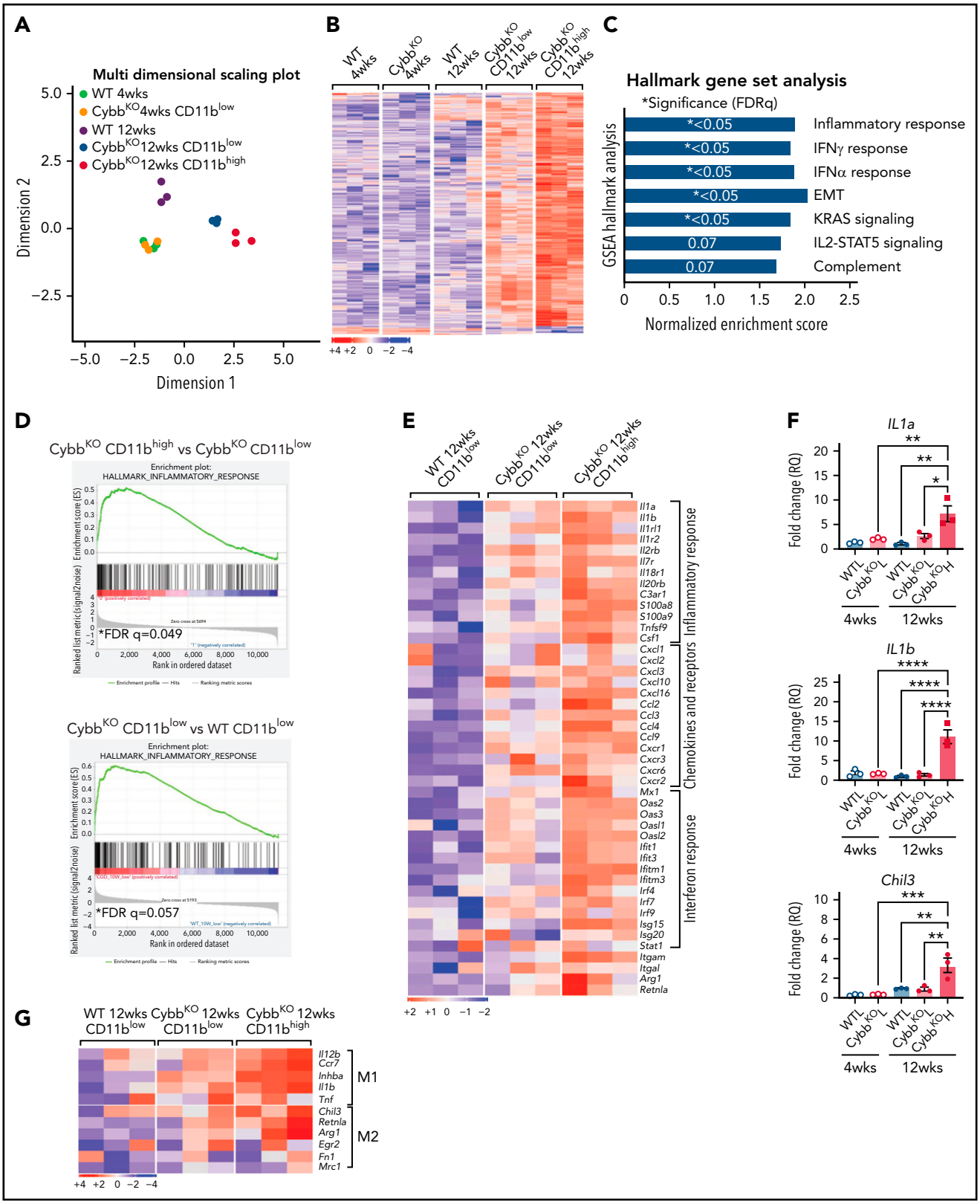

Figure 3. NOX2-deleted CD11b^{high} AMs acquire an inflammatory transcriptional signature. (A) Multidimensional scaling plot of RNA-seq transcriptomes in 2 different dimensions showing the differences in gene signatures among the indicated groups of samples of AMs sorted from 4- and 12-week-old mice (n = 3 independent samples in each group). (B) Heat maps showing relative expression of the top 500 altered genes in AMs in the different groups, as indicated (n = 3 independent samples in each group). (C) Hallmark gene sets with significant changes in GSEA between *Cybb*^{KO} CD11b^{high} and WT CD11b^{low} AMs from 12-week-old mice. False-discovery rate (FDR)q <0.05 was considered significant (n = 3 independent samples for each group). (D) GSEA plot showing differences in the hallmark inflammatory response gene sets between AMs from 12-week-old *Cybb*^{KO} CD11b^{high} and *Cybb*^{KO} CD11b^{low}, as well as *Cybb*^{KO} CD11b^{low} and WT CD11b^{low} mice, as indicated. FDRq <0.05 considered significant (n = 3 independent samples for each group). (E) Heat map from RNA-seq data showing relative expression of selected genes in *Cybb*^{KO} and WT

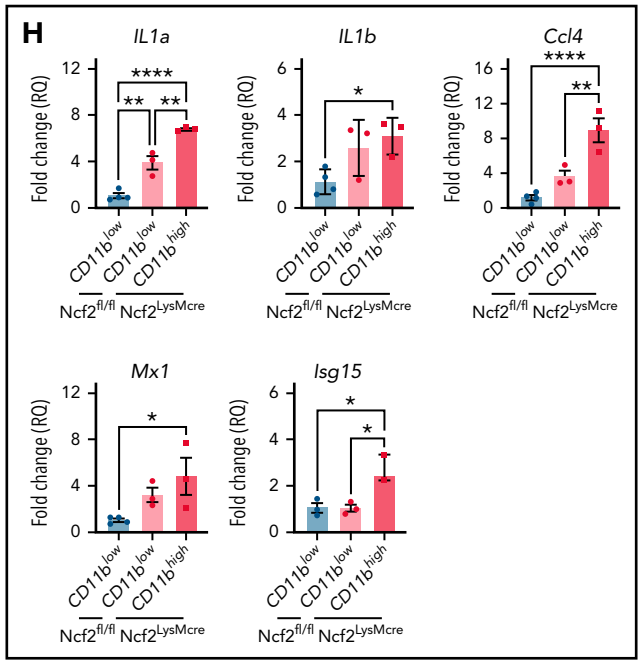

Figure 3 (continued) AMs from 12-week-old mice (n = 3 independent samples for each group). (F) qRT-PCR of gene expression in flow-sorted AMs from WT and *Cybb*^{KO} mice of different ages for selected genes. WTL, WT CD11b^{low} AM; *Cybb*^{KO} L, *Cybb*^{KO} CD11b^{low} AM; and *Cybb*^{KO} H, *Cybb*^{KO} CD11b^{high} AM (n = 3 samples for each group). (G) Heat map from AM RNA-seq data for selected M1 and M2 genes, as indicated. (H) qRT-PCR for expression of selected genes in flow sorted AMs, as indicated, from *Ncf2*$^{fl/fl}$ and Ncf2^{LysMcre} mice (n ≥ 3 samples for each group). Adjusted *P* values: **P* < .05; ***P* < .01; ****P* < .001. Bar graph data are expressed as the mean ± standard error of the mean. One-way analysis of variance was performed, followed by Tukey's post hoc analysis. **P* < .05; ***P* < .01; ****P* < .001; *****P* < .0001. FDR, false-discovery rate.

the monocyte marker CCR2 was not increased on CD11b^{high}AMs in *Cybb*^{KO} mice (supplemental Figure 1C-D), suggesting that these were not derived from very recently emigrated monocytes.[37] *Cybb*^{KO} AMs showed similar levels of annexin V staining and bromodeoxyuridine incorporation relative to WT AMs, even within the CD11b^{high} population (supplemental Figure1E-F). Thus, 12-week-old *Cybb*^{KO} mice develop an additional population of AMs that are CD11b^{high}, which could be derived from either resident AMs or bone marrow, but this process is not associated with increased apoptosis or turnover of AMs.

We also observed eosin-staining YM1 crystals within alveoli and AMs of 12-week-old *Cybb*^{KO} mice, accompanied in some mice by patchy intra-alveolar infiltrates (Figure 1G; supplemental Figure 2B), similar to NCF1-deleted CGD mice.[9,10] YM1 is a secreted chitinaselike protein (CLP) that easily forms crystals, often seen in the lungs of mice with various inflammatory conditions.[9,10,38,39] Notably, transcripts for CLPs CHIL1, CHIL3, CHIL4, and proteins related to their secretion were elevated in CD11b^{high} AMs from 12-week-old *Cybb*^{KO} mice, consistent with an activated AM phenotype (supplemental Figure 2C).

Thus, by the time CGD mice reach adulthood, absence of NOX2 activity leads to spontaneous development of an activated CD11b^{high} AM subset and an increase in alveolar neutrophils, proinflammatory cytokines, and YM1 crystals, all consistent with the dysregulation of alveolar homeostasis.

Deletion of NOX2 preferentially in macrophages is sufficient for an inflammatory lung phenotype

We next tested whether inactivating NOX2 primarily in macrophages is sufficient to cause the low-grade alveolar inflammation observed in germline loss-of-function mice. We crossed mice with a conditional *Ncf2* loss-of-function allele (*Ncf2*$^{fl/fl}$) to *LysM-Cre* mice[40] (supplemental Figure 3A). In the resulting *Ncf2*^{LysMCre} mice, ~95% of AMs or RPMs lacked NOX2 enzyme activity (supplemental Figure 3B-C), and NCF2 protein was not detected in RPM lysates (supplemental Figure 3D-E). However, NCF2 expression was only partially reduced in *Ncf2*^{LysMCre} neutrophils (supplemental Figure 3D-E). Peripheral blood neutrophils from *Ncf2*^{LysMCre} mice had either partial or near normal NOX2 activity by flow cytometry assay and superoxide production by quantitative cytochrome *c* reduction assay was ≈50% of *Ncf2*$^{fl/fl}$(supplemental Figure 3F-G). *Ncf2*^{LysMCre} monocytes harvested from marrow and peripheral blood had normal NCF2 expression and NOX2 activity (supplemental Figure 3D-E,H).

Although complete loss of NOX2 activity was restricted to macrophages, *Ncf2*^{LysMCre} mice developed inflammatory changes in the lungs similar to CGD mice. BAL from naive *Ncf2*^{LysMCre} mice at 12 week of age showed increased total leukocytes, neutrophils, and proinflammatory cytokines (Figure 2A-B) and a population of CD11c^{high}Siglec F^{high}CD11b^{high} AMs (Figure 2C). *Ncf2*^{LysMCre} mice also had increased transcripts for YM1 (supplemental Figure 2D) and crystals in alveoli and within AMs (Figure 2D; supplemental Figure 2B). Both *Ncf2*^{LysMCre} and *Cybb*^{KO} mice continued to exhibit CD11b^{high} AMs after 1 year of age, but *Ncf2*^{LysMCre} mice did not develop the focal alveolar infiltrates often seen in *Cybb*^{KO} mice, which also were sometimes larger in aging *Cybb*^{KO} mice (supplemental Figure 3I-K). We conclude that, although infiltrate formation most likely requires cross talk with other leukocytes entirely lacking NOX2, deletion of *Ncf2* restricted to macrophages is sufficient to produce an inflammatory alveolar environment in *Ncf2*^{LysMCre} mice.

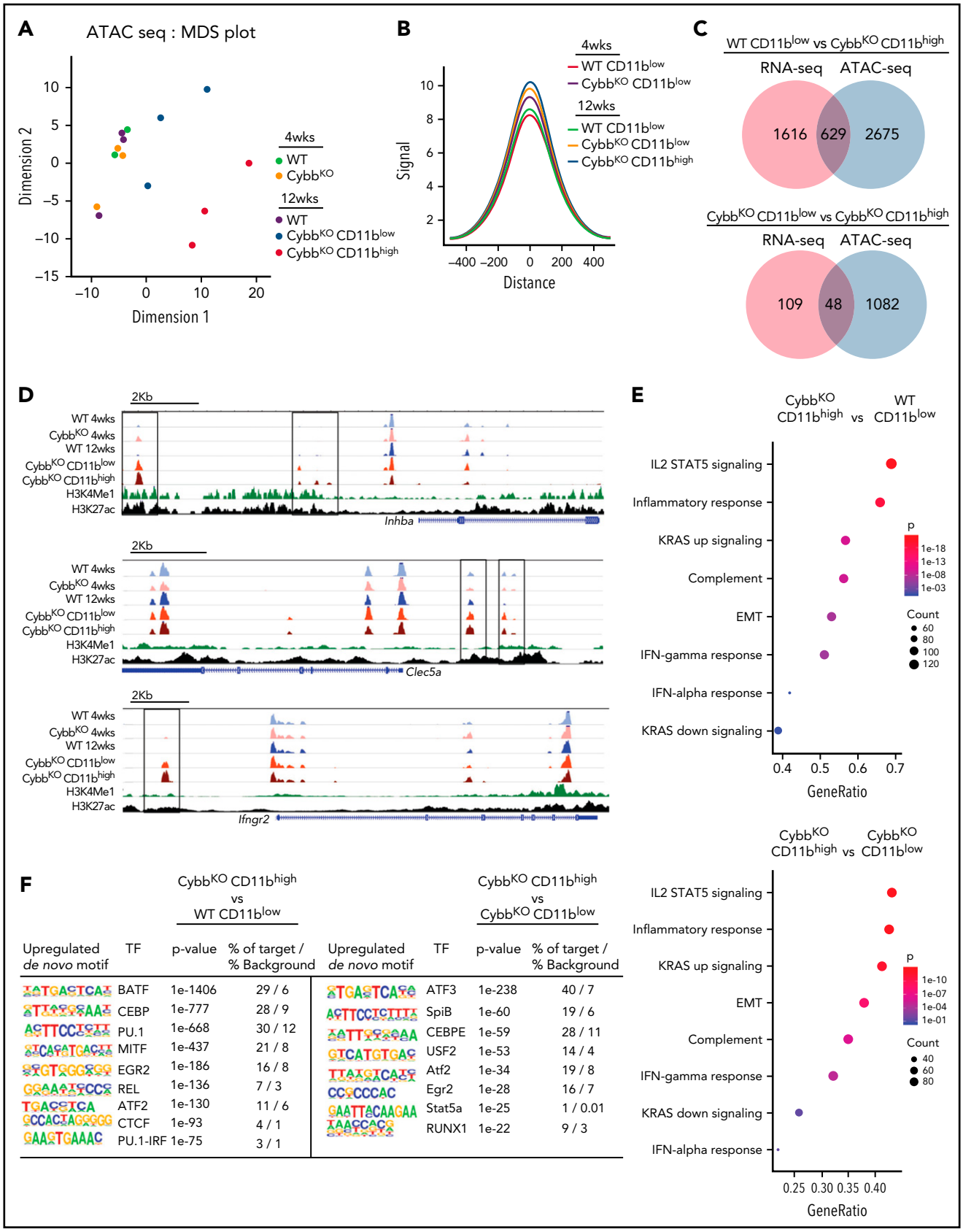

Figure 4.

We also studied female *Cybb* carrier mice, where approximately half of the leukocytes were NOX2^{+}, and half lacked NOX2 because of X-linked inactivation. Interestingly, ≈10% AMs from *Cybb* carriers harbored intracellular YM1 crystals by electron microscopy (supplemental Figure 2B), which could be a sign of increased AM activation; however, this fraction is much lower than that for *Cybb*^{KO} and *Ncf2*^{LysMCre} AMs, where ≈65% contain YM1 crystals detected by electron microscopy. Rare neutrophils were also seen in carrier BAL samples. Notably, carrier females did not develop evidence of lung inflammation by histology, CD11b^{high} AMs or increased BAL proinflammatory cytokines, even after 1 year of age (not shown), which suggests that there may be a threshold number of NOX2^{-} cells needed to promote spontaneous inflammatory changes in the alveolar environment.

Cytometry by time of flight for cell surface expression of canonical AM markers confirmed the presence of a CD11b^{high} population of CD11c^{high}Siglec F ^{high} AMs in *Ncf2*^{LysMCre} and *Cybb*^{KO} mice that was absent in WT mice (Figure 2E; supplemental Figure 4A-B). There was a modest decrease in CD64 in CD11b^{high} AMs, of uncertain biologic significance, along with a modest increase in CX3CR1. However, characteristic expression of other markers (F4/80, Siglec F, CD274, CD206, and MHCII [I-A/I-E]) (supplemental Figure 4B) were unaltered. Additional cytometry by time of flight results showed that *Ncf2*^{LysMCre} and *Cybb*^{KO} mice had small but significant decreases in lung B lymphocytes and natural killer cells compared with WT, but the percentages of alveolar and interstitial macrophages, dendritic cells, monocytes, eosinophils, and T lymphocytes were similar among all 3 genotypes (supplemental Figure 4C).

Transcriptomic profiles of AMs but not RPMs from NOX2-deleted mice showed an inflammatory signature

To gain insights into how CD11b^{high} AMs from NOX2-deficient mice differ from other AMs, we profiled gene expression of sorted AMs using RNA-seq. Multidimensional scaling analysis showed that AMs from 4-week-old WT and *Cybb*^{KO} mice share a similar gene expression signature (Figure 3A). However, in 12-week-old mice, the transcriptome of *Cybb*^{KO} AMs diverged from WT AMs, with differences between CD11b^{low} and CD11b^{high} *Cybb*^{KO} AMs. Differences are also depicted in a heat map showing the top 500 altered genes among various groups (Figure 3B) and n Venn diagrams (supplemental Figure 5A). We used gene set enrichment analysis (GSEA) of Hallmark gene sets[41] to interrogate the 2 most divergent groups: WT CD11b^{low} AMs and *Cybb*^{KO} CD11b^{high} AMs from 12-week-old mice. The inflammatory response gene set is among the most significantly different, along with IFN-α and IFN-γ responses, EMT and KRAS signaling (Figure 3C). The inflammatory response was the only gene set significantly altered between CD11b^{low} and CD11b^{high} AMs from 12-week-old *Cybb*^{KO} mice and also approached significance for CD11b^{low} AMs from 12-week-old *Cybb*^{KO} and WT mice (Figure 3D). Although no significant differences in GSEA were identified between CD11b^{low} AMs from *Cybb*^{KO} mice at the 2 ages, many of the upregulated genes in the 12-week-old samples are related to inflammation (supplemental Figure 5B). Relative expression of various activation-associated genes in AMs from 12-week-old mice are shown in Figure 3E. *IL1a*, *IL1b*, and *Chil3* expression were verified among various groups by qRT-PCR (Figure 3F). The skewed transcriptome in NOX2-deleted AMs did not correlate with polarization to either classic (M1) or alternative (M2) macrophage activation (Figure 3G), typical of diversity seen in vivo.[16] Finally, AMs sorted from *Ncf2*^{LysMCre} mice showed increased expression of *IL1a*, *IL1b*, *Ccl4, Mx1*, and *Isg15*, as compared with *Ncf2*$^{fl/fl}$ mice, especially in CD11b^{high} AMs (Figure 3H). In aggregate, these results indicate that the AM transcriptome becomes skewed toward a more proinflammatory profile as mice with either global or macrophage deletion of NOX2 reach adulthood, with these changes most pronounced in the CD11b^{high} AM population.

To investigate whether there is tissue specificity to resident macrophage remodeling with age in CGD mice, we analyzed gene expression in RPMs by RNA microarray. We sorted the 2 groups of RPMs (B220^{-}CD115^{+}F4/80^{high}MHCII^{-} and B220^{-}CD115^{+}F4/80^{low}MHCII^{high}) from naive 12-week-old WT and *Cybb*^{KO} mice. Although the 2 subtypes of RPMs were shown to be clearly different from each other by principal component analysis, WT and *Cybb*^{KO} macrophages were similar, and within each RPM subgroup, expression of hallmark gene sets was similar between WT and *Cybb*^{KO} (supplemental Figure 5C-D). These results show that the impact of NOX2 deletion on the remodeling of the resident macrophage transcriptome at homeostasis is influenced by the tissue niche.

Chromatin profiles reveal epigenetic changes in CD11b^{high} AMs in *Cybb*^{KO} mice

Epigenetic modifications of the enhancer landscape and their plasticity play an important role in regulating macrophage gene expression.[15,22] To interrogate differences in the epigenome of WT and CGD AMs, we performed ATAC-seq. A multidimensional scaling plot showed distinct differences among groups by genotype and age (Figure 4A). AMs from 4-week-old WT and *Cybb*^{KO} mice and 12-week-old WT mice had similar ATAC-seq profiles, but AMs from 12-week-old *Cybb*^{KO} mice were distinct, particularly the CD11b^{high} subpopulation (Figure 4A). CD11b^{high} AMs had a higher number of ATAC-seq peaks compared with CD11b^{low}AMs from 12-week-old mice of either genotype, as did AMs from 12-week-old *Cybb*^{KO} mice compared with those from

Figure 4. NOX2-deleted AMs acquire epigenetic alterations. (A) An MDS plot of AM ATAC-seq peak signals in 2 different dimensions showing differences among the indicated groups of mice (n = 3 independent samples in each group). (B) Histogram comparing aggregate ATAC-seq peak heights around TSSs (±500 kb) in various groups for the genes with significant differences between *Cybb*^{KO} CD11b^{high} AMs and WT CD11b^{low} AMs from 12-week-old mice. (C) Venn diagram showing the overlay of genes with significant alterations in both RNA-seq and ATAC-seq (TSS, ±500 kb) among various groups. (D) Representative WUSTL epigenome browser tracks displaying normalized ATAC-seq peak signal distribution in selected genes from AMs sampled from the indicated groups of 4- and 12-week-old WT and *Cybb*^{KO} mice along with CHIP-seq data for H3K4Me1 and H3K27ac marks from Lavin et al.[58] Boxes indicate ATAC-seq peaks that are significantly different in 12-week-old *Cybb*^{KO} samples compared with 12-week-old WT samples. (E) Hallmark gene set analysis for genes with altered ATAC-seq peak signals between *Cybb*^{KO} CD11b^{high} and WT CD11b^{low} as well as *Cybb*^{KO} CD11b^{high} and *Cybb*^{KO} *CD11b*^{low}AMs. (F) HOMER de novo motif enrichment analysis for transcription factor binding sites in open chromatin ±500 kb from the TSS, as identified in ATAC-seq, as analyzed in AMs sampled from 12-week-old mice (n = 3 independent samples in each group). The percentage of motif occurrence in peaks vs background is also shown. CHIP, chromatin immunoprecipitation; HOMER, hypergeometric optimization of motif enrichment; MDS, multidimensional scaling; TSS, transcription start site.

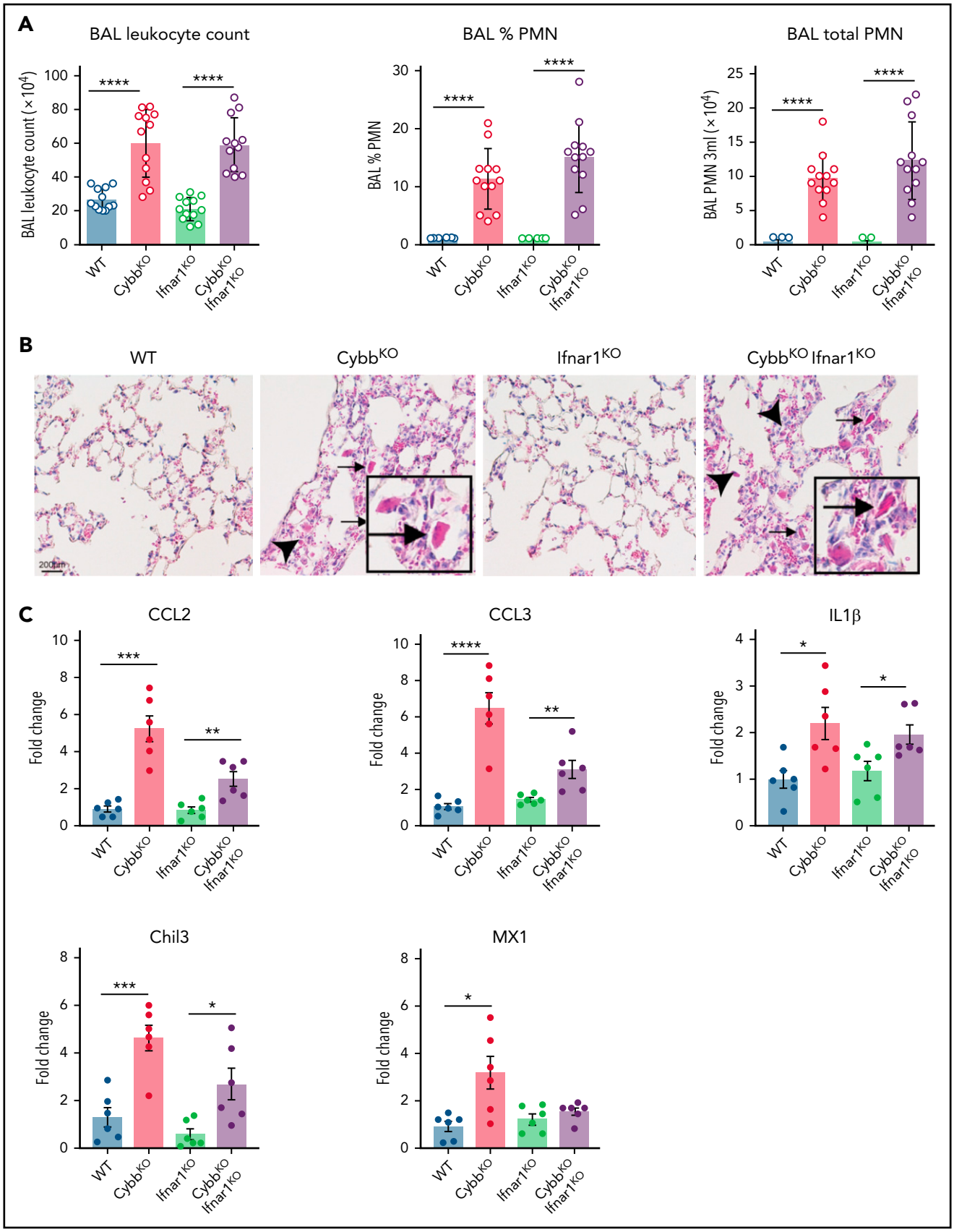

Figure 5.

younger *Cybb*^{KO} mice (supplemental Figure 5E). Analysis of aggregate peak heights showed increased chromatin accessibility in *Cybb*^{KO} AMs compared with WT, with CD11b^{high} AMs from 12-week-old *Cybb*^{KO} mice having the greatest difference (Figure 4B). These results indicate that the AM epigenome in NOX2-deficient mice changes between 4 and 12 weeks after birth and acquires a more open chromatin state compared with WT AMs.

We next explored possible implications of increased chromatin accessibility in *Cybb*^{KO} AMs for gene expression. Many of the genes with increased RNA expression in *Cybb*^{KO} CD11b^{high} AMs showed increased accessibility (Figure 4C-D), which could contribute to their increased transcription. We also investigated the association of differential ATAC-seq signals with GSEA, focusing on gene sets with significant differences (Figure 3C). Six of 8 of these sets showed significant difference in chromatin accessibility in *Cybb*^{KO} CD11b^{high} AMs compared with either WT AMs or *Cybb*^{KO} CD11b^{low} AMs from 12-week-old mice (Figure 4E). HOMER (hypergeometric optimization of motif enrichment) analysis showed that the transcription factor motifs most significantly enriched in open chromatin regions in CD11b^{high} AMs included those capable of binding to members of the basic helix-loop-helix leucine family (ATF, BATF, USF2, and MITF) or to transcription factors that play prominent roles in myeloid lineage determination and are enriched in macrophage enhancer regions (Pu.1, CEBP, and RUNX; Figure 4F).[21,22,42] NFKB/REL and Stat binding sites were also enriched in *Cybb*^{ko}CD11b^{high} AMs. The increased accessibility of myeloid lineage enhancers and of the other motifs are consistent with the upregulated proinflammatory gene expression in NOX2-deleted CD11b^{high} AMs.

Development of lung inflammation in *Cybb*^{ko} mice does not require host microbiota or the type I IFN receptor

As ongoing exposure to either environmental or host-associated microbes could contribute to the development of alveolar inflammation, we examined the impact of raising *Cybb*^{KO} mice under germ-free conditions. Although there was a small but significant decrease in BAL neutrophils, CD11b^{high} AMs were not reduced compared with *Cybb*^{KO} mice maintained in specific-pathogen–free housing (supplemental Figure 6A). Germ-free *Cybb*^{KO} mice also had eosinophilic AM and YM1 crystals within alveoli (supplemental Figure 6B). Although mice could still be exposed to sterile microbe–derived substances, such as in food or bedding, the presence of host microbiota or microbes in the environment are not necessary for NOX2-deleted animals to develop altered alveolar homeostasis.

Enhanced leukocyte expression of type I IFN response genes can be induced by viral or bacterial molecular patterns, as well as other inflammatory stimuli. Increased IFN response genes are reported in humans who lack functional NOX2 and in CGD mice, even in germ-free conditions, which may reflect exposure to nonpathogenic viruses or to sterile proinflammatory molecules.[43] Our results showed a significant upregulation in IFN-α response genes in NOX2-deleted CD11b^{high} AMs (Figure 3C,E,H) and higher BAL levels of IFN-α (supplemental Figure 2A). To test whether type I IFN drives lung inflammation in NOX2-deleted mice, we studied *Ifnar1*$^{-/-}$*Cybb*^{KO} (DKO) mice.[27] Lungs of DKO mice displayed inflammatory changes, including increased BAL neutrophils and YM1 crystals (Figure 5A-B). Transcripts for Chil3 (YM1) and proinflammatory cytokines IL-1β, CCL2, and CCL3 were significantly increased in BAL macrophages from both *Cybb*^{KO} and DKO mice compared with littermates that retained a WT *Cybb* allele (Figure 5C). Thus, IFNAR1 signaling is not necessary for *Cybb*^{KO} mice to develop spontaneous lung inflammation.

NOX2^{-} AMs, but not RPMs, have increased responses to TLR agonists

We reasoned that the proinflammatory changes in AMs lacking NOX2 may be associated with a cell-intrinsic hyperreactivity to inhaled materials in the environment or debris that AMs continuously manage during homeostasis. To approach this question, we used agonists of Toll-like receptor-2 (TLR2) and TLR4, which can detect DAMPS and exogenous substances in addition to bacterial and fungal cell walls.[44-46] We stimulated AMs isolated from *Ncf2*^{KO} and WT mice of different ages with either Pam3CSK4 or LPS and analyzed gene expression. In AMs harvested from 4-week-old mice, LPS induced significantly higher *Il1b*, *Ccl3*, and *Ccl4* expression in *Ncf2*^{KO} AMs compared with *Ncf2*$^{fl/fl}$ (Figure 6A). Hence, AM reactivity was elevated at a young age, when basal transcriptional and ATAC-seq profiles are similar to WT mice. *Ncf2*^{KO} AMs from 12-week-old mice additionally showed significantly increased responses to Pam3CSK4 compared with WT AMs, as well as to LPS (Figure 6B). Notably, AMs from 12-week-old *Ncf2*^{LysMCre} mice were also hyperresponsive to Pam3CSK4 or LPS (Figure 6C). Finally, to investigate whether the macrophage tissue niche influenced this hyperresponsive phenotype, we performed similar studies on RPMs from 12-week-old WT and *Cybb*^{KO} mice, but there were no differences between genotypes after stimulation with either Pam3CSK4 or LPS (supplemental Figure 7). In aggregate, these results show the importance of AM NOX2 activity for limiting their reactivity, and that cell-extrinsic factors related to their tissue niche are also important.

Increased lung inflammation after remote tissue inflammation in NOX2-inactivated mice correlates with proinflammatory remodeling of AMs

We next examined whether the age-dependent priming of AMs lacking NOX2 that develops under basal conditions leads to amplified responses to inflammatory insults. We first examined lung inflammation induced by sterile fungal cell walls, which elicit increased neutrophilic infiltration in adult CGD mice.[28,47,48] At 18 h after lung instillation of zymosan, both 4- and 12-week-old *Cybb*^{KO} mice displayed a significantly greater number of

Figure 5. Type I IFN signaling is not necessary for NOX2-deleted mice to develop spontaneous lung inflammation and activated AMs. (A) BAL leukocyte count, percentage of polymorphonuclear leukocytes (PMNs), and total PMNs in 3 mL of BAL from WT, *Cybb*^{KO}, *Ifnar1*^{KO}, and *Cybb*^{KO} *Ifnar1*^{KO} mice (n = 12 in each group). (B) Hematoxylin-eosin–stained lung tissues showing the presence of eosinophilic macrophages (arrowhead) and extracellular crystals (arrow) in *Cybb*^{KO} and *Cybb*^{KO}*Ifnar1*^{KO} mice. Scale bar, 200 μm and the scale is same for all panels. Representative image from more than 4 samples in each group. (C) qRT-PCR analysis of gene expression in BAL cells isolated from WT, *Cybb*^{KO}, *Ifnar1*^{KO}, and *Cybb*^{KO}*Ifnar1*^{KO} mice (n = 6 in each group). Bar graph data are expressed as the mean ± standard error of the mean. Experiments were repeated at least twice and the Student *t* test was performed for samples distributed between 2 groups. *$P < .05$; **$P < .01$; ***$P < .001$; ****$P < .0001$.

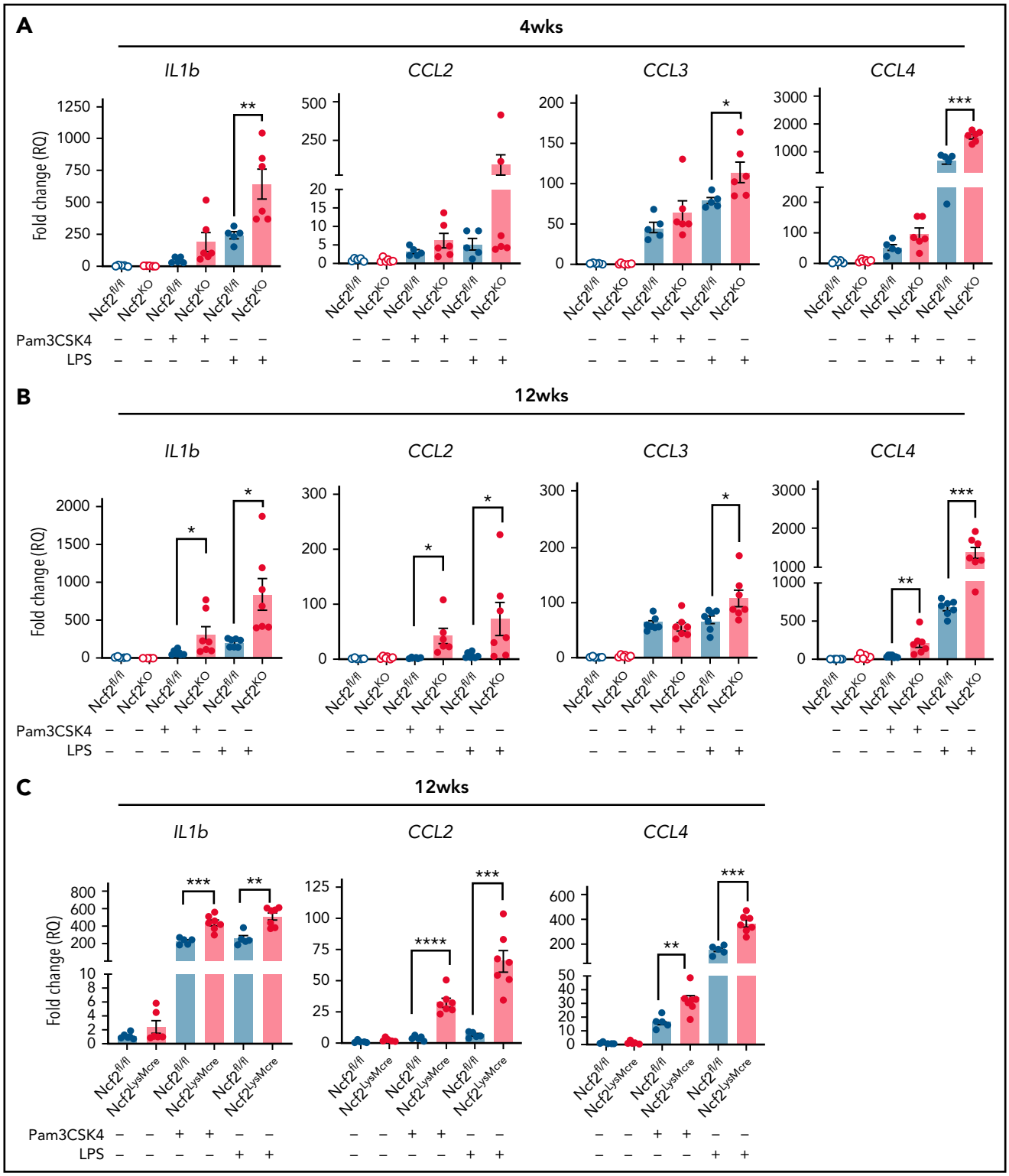

Figure 6. AMs from mice with global or LysMCre-mediated deletion of NOX2 have increased responses to TLR stimulation. (A-B) AMs isolated from BAL of *Ncf2*$^{fl/fl}$ and *Ncf2*^{KO} mice were stimulated with Pam3CSK4 or LPS, and gene expression was assayed by qRT-PCR in 4-week-old (A) and 12-week-old (B) mice. (C) AMs isolated from BAL of 12-week-old *Ncf2*$^{fl/fl}$ and *Ncf2*^{LysMCre} mice were stimulated with Pam3CSK4 or LPS, and gene expression was assayed by qRT-PCR. Bar graph data are expressed as the mean ± standard error of the mean. Experiments were repeated at least twice. The Student *t* test was performed for samples distributed between 2 groups. *$P < .05$; **$P < .01$; ***$P < .001$; ****$P < .0001$.

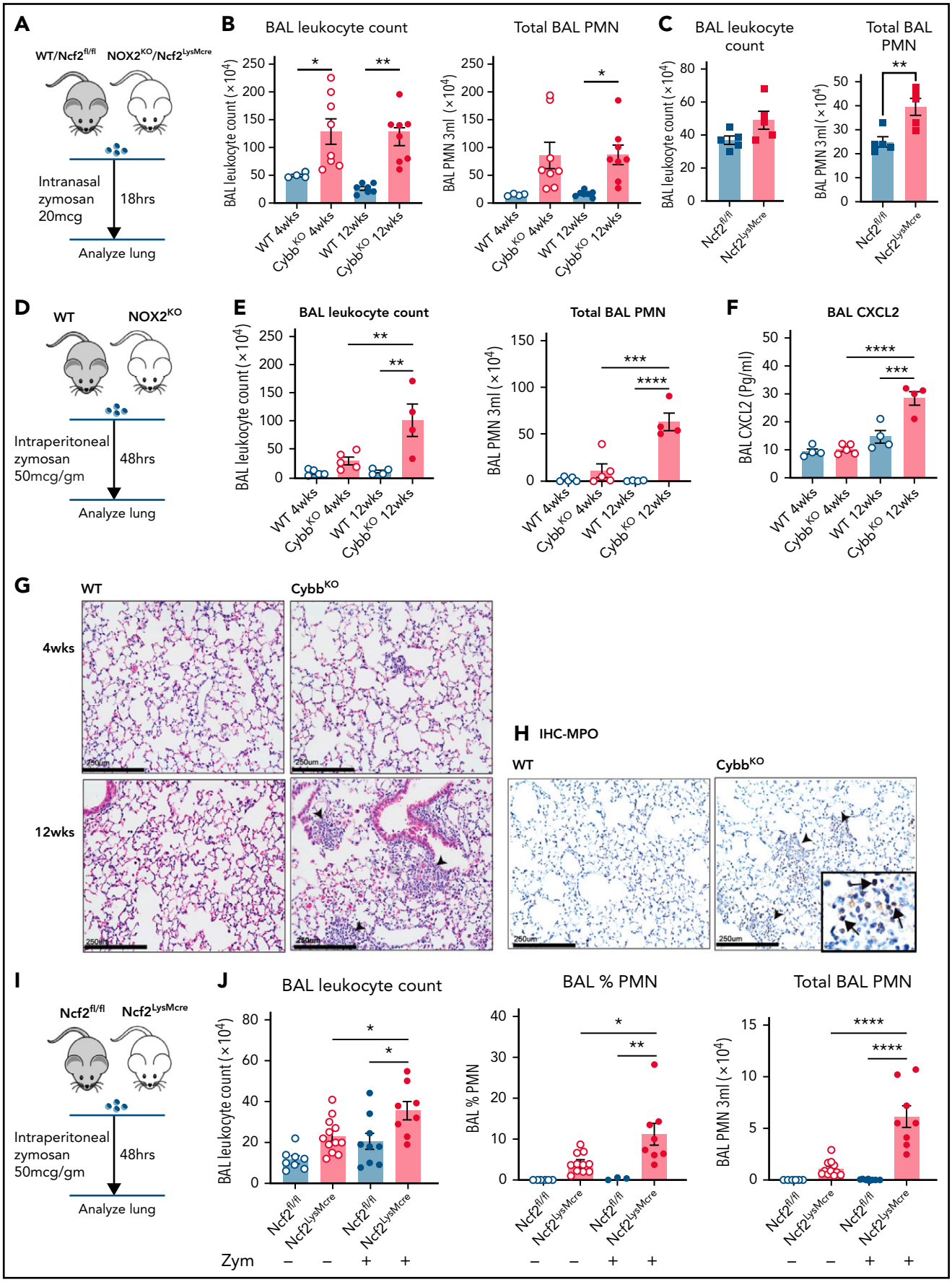

Figure 7.

BAL neutrophils compared with WT mice (Figure 7A-B). Thus, the hyperinflammatory response of NOX2-inactivated mice to direct lung challenge with zymosan is age independent. We next investigated responses of mice at different ages to indirect lung injury induced by remote tissue inflammation (Figure 7D). We modified a peritoneal zymosan-induced systemic inflammatory response syndrome model,[29,30,49,50] using a ≈10-fold lower dose of zymosan to avoid mortality. This dose elicited significantly greater neutrophilic inflammation in the peritoneal cavity of *Cybb*^{KO} compared with WT mice at both 4 and 12 wk of age (supplemental Figure 8A-B). However, only 12-week-old *Cybb*^{KO} mice had a significantly increased number of BAL neutrophils, focal lung neutrophil infiltrates, and elevated BAL CXCL2 at 48 hours after induction of peritonitis, whereas neither 4-week-old *Cybb*^{KO} nor WT mice developed evidence of lung inflammation (Figure 7D-H).

We next investigated whether LysMCre-mediated deletion of NOX2 activity resulted in altered responses to inflammatory challenges. Twelve-week-old *Ncf2*^{LysMCre} mice had a significantly increased number of BAL neutrophils after lung instillation of zymosan compared with *Ncf2*$^{fl/fl}$ littermates, although the number of neutrophils was about twofold less than that in CGD mice (Figure 7B-C). Zymosan-induced peritoneal inflammation was similar in *Ncf2*$^{fl/fl}$ and *Ncf2*^{LysMCre} mice (supplemental Figure 8C-D), indicating that deletion of NOX2 preferentially in macrophages does not enhance the peritoneal response to zymosan. However, the peritoneal inflammation was still accompanied by pulmonary inflammation in *Ncf2*^{LysMCre} mice at 48 h, with increased BAL leukocytes and neutrophils compared with baseline or to *Ncf2*$^{fl/fl}$ controls (Figure 7I). Inflammatory changes in the BAL were milder compared with CGD mice, which most likely reflects the more modest inflammatory response to peritoneal zymosan in *Ncf2*^{LysMCre} mice.

Collectively, these results show that the proinflammatory remodeling of lung AMs and dysregulated alveolar homeostasis in mice with either global or macrophage NOX2 inactivation can result in increased lung inflammation triggered by distant tissue inflammation.

Discussion

Dysregulated inflammatory responses provoked by even noninfectious stimuli is a hallmark of the inherited deficiency of NOX2. In this study, we identified a pivotal anti-inflammatory role of NOX2 in AMs in maintaining alveolar homeostasis. Utilizing genetic models, we showed that mice with NOX2-deleted AMs spontaneously acquire changes in the transcriptome and epigenome over the first few months of life. This remodeling is skewed toward increased chromatin accessibility of motifs for activating transcription factors and expression of genes associated with the inflammatory response, particularly in an activated AM subset distinguished by increased CD11b expression. This is accompanied by low-level inflammatory changes in the alveoli at baseline, including increased proinflammatory cytokines and YM1 and the presence of neutrophils. These changes are also associated with increased inflammation evoked by distant tissue inflammation. Remarkably, although NOX2 is also highly expressed in neutrophils and monocytes, loss of NOX2 activity restricted to AMs is sufficient to elicit similar findings.

Our data show that AM NOX2 attenuates inflammation during homeostasis, which also sets a threshold for responses to insults. Multiple contributing factors are most likely involved in this NOX2-dependent remodeling process. Given their anatomic location as airway sentinels, we speculate that the changes in NOX2-inactivated mice are, at least in part, linked to dysregulated AM activation triggered by ongoing exposure to inhaled materials and clearance of debris that leads to remodeling of the basal AM transcriptome and epigenome. Although our studies using germ-free mice eliminated the involvement of living microorganisms, NOX2 limited cell-intrinsic AM activation to ligands for TLR2 and TLR4, which are receptors that can detect sterile microbial ligands, DAMPs, and exogenous substances.[44-46] This hyperresponsiveness could, in part, reflect impaired redox-mediated damping of NFκB transcriptional activity reported for NOX2-deleted lung macrophages.[51] Amplified type I IFN-initiated signaling is proposed to contribute to dysregulated inflammation in NOX2 deficiency.[43] However, our studies of IFNAR1-deleted CGD mice indicate that the enhanced expression of IFN-α signature genes in CD11b^{high} AMs lacking NOX2 is a downstream consequence rather than a driver of proinflammatory changes in the lung. In addition, the altered resident macrophage phenotype in the absence of NOX2 was tissue specific, as these changes were seen in AMs but not in RPMs, which confirms and substantially extends prior work.[31,50] Underlying mechanisms for this tissue specificity remain to be clarified, but may reflect epigenetic and transcriptional features of AMs that enable them to otherwise maintain a relatively tolerogenic state in their tissue niche. Finally, epithelial cells in the airways and alveoli produce and release hydrogen peroxide via the NADPH oxidases DUOX1 and DUOX2,[52] but this process does not complement the loss of NOX2. We speculate that because deficiency of intracellular ROS is the likely culprit in deregulating AMs lacking NOX2,

Figure 7. Lung inflammation induced by zymosan challenge or remote tissue inflammation in mice with global or LysMCre-mediated deletion of NOX2. (A) Schema for zymosan-induced lung inflammation in WT or *Ncf2*$^{fl/fl}$ and *Cybb*^{KO} (NOX2^{KO}) or *Ncf2*^{LysMcre} mice. (B) BAL leukocyte counts and total polymorphonuclear leukocytes (PMNs), as identified by microscopy in 3 mL of BAL from WT and *Cybb*^{KO} mice of different ages after intranasal administration of zymosan (n ≥ 4 mice in each group). (C) BAL leukocyte counts and total PMNs as identified by microscopy in 3 mL of BAL from *Ncf2*$^{fl/fl}$ and *Ncf2*^{LysMcre} mice with different ages following intranasal administration of zymosan (n ≥ 5 mice in each group). (D) Schema for analysis of lung inflammation after intraperitoneal administration of zymosan in WT and *Cybb*^{KO} mice. (E) BAL leukocytes, and total PMNs in 3 mL of BAL from the indicated groups of WT and *Cybb*^{KO} mice of different ages after intraperitoneal zymosan (n ≥ 4 mice in each group). (F) BAL CXCL2 levels in samples from the indicated groups after intraperitoneal zymosan (n ≥ 4 mice in each group). (G) Hematoxylin-eosin staining of lung tissues from WT and *Cybb*^{KO} mice after intraperitoneal zymosan. Representative image from 1 of 4 samples in each group. Arrowheads, focal neutrophil infiltrates. Scale bar, 250 μm. (H) Representative images of immunohistochemistry for MPO to identify lung PMNs after intraperitoneal zymosan. Arrows, MPO^{+} cells. Representative image from 4 samples of each group. Scale bars, 250 μm. (I) Schema for analysis of lung inflammation after intraperitoneal zymosan in 12-week-old *Ncf2*$^{fl/fl}$ and *Ncf2*^{LysMCre} mice. (J) BAL leukocyte counts, percentage of PMNs by microscopy, and total PMNs in 3 mL of BAL from naive (data also shown in Figure 2A) or zymosan-challenged *Ncf2*$^{fl/fl}$ and *Ncf2*^{LysMCre} mice. Bar graph data are expressed as the mean ± standard error of the mean. Experiments were repeated at least twice. The Student *t* test was performed to compare results between each genotype for each age group in panel B. *$P < .05$; **$P < .01$. One-way analysis of variance was performed followed by Tukey's post hoc analysis for data (E-F,J). *$P < .05$; **$P < .01$; ***$P < .001$; ****$P < .0001$.

DUOX1/2-derived cell-extrinsic ROS are not effective because of the limitations on the amounts and/or availability for regulating intracellular macrophage processes.

NOX2-deleted AMs underwent epigenetic changes in the enhancer landscape, including increased accessibility of motifs for myeloid lineage enhancers and other transcription factors that increase responses of associated immune genes to stimulation. These acquired changes in NOX2-deleted AMs could be considered a type of learned or trained immunity, a facet of innate immunity that has attracted much recent attention.[21,53] Epigenetic and functional alterations in AMs have previously been described after lung infection, either in residential AMs or in recently emigrated monocyte-derived AMs, although the underlying mechanisms that guide their reprograming remain incompletely understood.[12,34,37,54-57] These changes are associated with either increased immunoreactivity of AMs or suppressive effects, depending on the inciting insult. In contrast, the changes in the epigenome of NOX2-deleted AMs develop under basal conditions in the first months of life.

This study provides new insights into the impact of NOX2 on macrophage function and the pathologic consequences of its absence for lung homeostasis and potentially other organs, which has clinical relevance for patients with CGD. Inflammatory lung disease is a poorly understood but serious complication that develops in many adult patients with CGD and can lead to reduced diffusion capacity and progressive hypoxia.[3-8] Although difficult to treat, according to anecdotal reports, the inflammatory lung disease can be reversed by allogeneic hematopoietic stem cell transplantation.[3] Its pathogenesis is poorly understood but does not always appear to be a consequence of prior lung infections. Computed tomography findings are variable and include interstitial or micronodular infiltrates.[3-5] Biopsy studies in patients without intercurrent infections are very limited, but have shown variable findings of neutrophil infiltrates, bronchiolitis, or fibrosis.[5] It is unknown whether any features of the lung disease that develops in NOX2-deleted mice overlap those in patients with CGD. However, we hypothesize that loss of NOX leads to hyperinflammatory resident AMs and an alveolar environment that predisposes to lung inflammation in patients with CGD as a consequence of direct or indirect events. This could affect outcomes, even with lung pathogens not associated with increased microbial virulence per se in CGD, such as viruses, *Streptococcus pneumonia*, or mycoplasma, and it could induce secondary lung inflammation with remote infections or injury. Whether the use of IFN-γ, which boosts phagocyte function and is currently used to reduce the incidence of infections in CGD,[1] or the use of agents blocking IL-1 signaling could reduce inflammatory lung disease in CGD may be of interest for future study.

In summary, our results identify a new role for NOX2 to modulate alveolar homeostasis by regulating sentinel AMs and suppressing remodeling of their epigenome and transcriptome to a more proinflammatory state. Both cell-intrinsic factors and their anatomic niche contribute to the acquisition of these changes in the absence of NOX2. This information may shed light on the pathogenesis of chronic lung inflammation that can develop in patients with CGD and may be helpful for the development of treatments to promote protective lung immune responses in general.

Acknowledgments

The authors thank Hongjie Gu for assistance with statistical analysis, Steve Van Dyken and Gwen Randolph for helpful discussions, Jeanette Pingel for early work in generating the NCF2 f/f mice, and Tina McGrath for assistance with manuscript preparation; the Washington University in St. Louis (WUSTL) Genome Technology Core (in part funded by an award from the Children's Discovery Institute of Washington University and St. Louis Children's Hospital) and the WUSTL Mouse Embryonic Stem Cell Core (affiliated with the Siteman Cancer Center at the time the work was performed), for providing embryonic stem cell culture services; the Mouse Genetics Core at Washington University St. Louis School of Medicine for their support with animal production and care; the Andrew M. and Jane M. Bursky Center for Human Immunology and Immunotherapy Programs (CHiiPs); and the Molecular Microbiology Imaging Core.

This study was supported by National Institutes of Health, National Heart, Lung, and Blood Institute grant R01HL140837 (M.C.D.), National Institute of Dental and Craniofacial Research grant R01 DE082896 (J.B.), and National Institute of General Medical Sciences grant GM125504; (J.B.); the Children's Discovery Institute (CDI) of Washington University, and St. Louis Children's Hospital (M.C.D.); a Leukemia and Lymphoma Scholar award (J.A.M.); and the Canadian Institutes of Health Research FDN 154329 (J.H.B). J.H.B. holds the Pitblado Chair in Cell Biology, and infrastructure for the J.H.B. laboratory was provided by a John Evans Leadership Fund grant from the Canadian Foundation for Innovation and the Ontario Innovation Trust.

Authorship

Contribution: S.B., R.A.I., J.D.R.M., W.L.B., J.J.A., J.H.B., J.B., J.A.M., and M.C.D designed the experiments; S.B., R.A.I., J.D.R.M., Y.L., G.H., W.L.B., J.J.A., and J.B. performed the experiments; S.B., R.A.I., W.Y., J.D.R.M., G.H., W.L..B, J.J.A, J.B., J.A.M., and M.C.D. analyzed the data; S.B., R.A.I., W.Y., Y.L., W.L.B., J.J.A., J.H.B., J.B., J.A.M., and M.C.D. interpreted the data; S.B., R.A.I., J.H.B., J.B., J.A.M., and M.C.D. contributed to writing the manuscript; and S.B. and M.C.D. wrote the manuscript.

Conflict-of-interest disclosure: The authors declare no competing financial interests.

ORCID profiles: S.B., 0000-0002-2101-4124; R.A.I., 0000-0002-7043-6630; W.Y., 0000-0001-8162-033X; J.D.R., 0000-0001-6385-030X; Y.L., 0000-0003-4396-0557; J.J.A., 0000-0001-9125-7968; J.H.B., 0000-0002-5802-7789; J.B., 0000-0001-6185-1915; J.A.M., 0000-0002-0766-4200; M.C.D., 0000-0002-7796-2908.

Correspondence: Mary C. Dinauer, Washington University School of Medicine, PO Box 8208, 660 S Euclid Ave, St. Louis, MO 63110; e-mail: mdinauer@wustl.edu.

Footnotes

Submitted 3 January 2022; accepted 2 March 2022; prepublished online on *Blood* First Edition 23 March 2022. DOI 10.1182/blood.2021015365.

Data for RNA microarray, RNA-seq, and ATAC-seq were deposited and available in GEO (accession number GSE198778).

Requests for data sharing may be submitted to Mary C. Dinauer (mdinauer@wustl.edu).

The online version of this article contains a data supplement.

There is a *Blood* Commentary on this article in this issue.

REFERENCES

1. Dinauer MC. Inflammatory consequences of inherited disorders affecting neutrophil function. *Blood*. 2019;133(20):2130-2139.
2. Dinauer MC. Primary immune deficiencies with defects in neutrophil function. *Hematology Am Soc Hematol Educ Program*. 2016;2016:43-50.
3. Campos LC, Di Colo G, Dattani V, et al. Long-term outcomes for adults with chronic granulomatous disease in the United Kingdom. *J Allergy Clin Immunol*. 2021; 147(3):1104-1107.
4. Dunogué B, Pilmis B, Mahlaoui N, et al. Chronic granulomatous disease in patients reaching adulthood: a nationwide study in France. *Clin Infect Dis*. 2017;64(6):767-775.
5. Salvator H, Mahlaoui N, Catherinot E, et al. Pulmonary manifestations in adult patients with chronic granulomatous disease. *Eur Respir J*. 2015;45(6):1613-1623.
6. Liese J, Kloos S, Jendrossek V, et al. Long-term follow-up and outcome of 39 patients with chronic granulomatous disease. *J Pediatr*. 2000;137(5):687-693.
7. Khaldi H, Marchand-Adam S, Kannengiesser C, et al. Diffuse interstitial pneumonia and pulmonary hypertension: a novel manifestation of chronic granulomatous disease. *Eur Respir J*. 2009;33(6):1498-1502.
8. Kawai T, Watanabe N, Yokoyama M, et al. Interstitial lung disease with multiple microgranulomas in chronic granulomatous disease. *J Clin Immunol*. 2014;34(8):933-940.
9. Liu Q, Cheng LI, Yi L, et al. p47phox deficiency induces macrophage dysfunction resulting in progressive crystalline macrophage pneumonia. *Am J Pathol*. 2009; 174(1):153-163.
10. Harbord M, Novelli M, Canas B, et al. Ym1 is a neutrophil granule protein that crystallizes in p47phox-deficient mice. *J Biol Chem*. 2002;277(7):5468-5475.
11. Garbi N, Lambrecht BN. Location, function, and ontogeny of pulmonary macrophages during the steady state. *Pflugers Arch*. 2017; 469(3-4):561-572.
12. Guilliams M, Svedberg FR. Does tissue imprinting restrict macrophage plasticity? *Nat Immunol*. 2021;22(2):118-127.
13. Kierdorf K, Prinz M, Geissmann F, Gomez Perdiguero E. Development and function of tissue resident macrophages in mice. *Semin Immunol*. 2015;27(6):369-378.
14. Amit I, Winter DR, Jung S. The role of the local environment and epigenetics in shaping macrophage identity and their effect on tissue homeostasis [published correction appears in *Nat Immunol*. 2017;18(2):246]. *Nat Immunol*. 2016;17(1):18-25.
15. Troutman TD, Kofman E, Glass CK. Exploiting dynamic enhancer landscapes to decode macrophage and microglia phenotypes in health and disease. *Mol Cell*. 2021;81(19):3888-3903.
16. Blériot C, Chakarov S, Ginhoux F. Determinants of resident tissue macrophage identity and function. *Immunity*. 2020;52(6): 957-970.
17. Chakarov S, Lim HY, Tan L, et al. Two distinct interstitial macrophage populations coexist across tissues in specific subtissular niches. *Science*. 2019;363(6432):eaau0964.
18. Gosselin D, Link VM, Romanoski CE, et al. Environment drives selection and function of enhancers controlling tissue-specific macrophage identities. *Cell*. 2014;159(6): 1327-1340.
19. Okabe Y, Medzhitov R. Tissue biology perspective on macrophages. *Nat Immunol*. 2016;17(1):9-17.
20. Lavin Y, Winter D, Blecher-Gonen R, et al. Tissue-resident macrophage enhancer landscapes are shaped by the local microenvironment. *Cell*. 2014;159(6): 1312-1326.
21. Natoli G, Ostuni R. Adaptation and memory in immune responses. *Nat Immunol*. 2019; 20(7):783-792.
22. Glass CK, Natoli G. Molecular control of activation and priming in macrophages. *Nat Immunol*. 2016;17(1):26-33.
23. Mowat AM, Scott CL, Bain CC. Barrier-tissue macrophages: functional adaptation to environmental challenges. *Nat Med*. 2017; 23(11):1258-1270.
24. Hussell T, Bell TJ. Alveolar macrophages: plasticity in a tissue-specific context. *Nat Rev Immunol*. 2014;14(2):81-93.
25. Pollock JD, Williams DA, Gifford MA, et al. Mouse model of X-linked chronic granulomatous disease, an inherited defect in phagocyte superoxide production. *Nat Genet*. 1995;9(2):202-209.
26. Jacob CO, Yu N, Yoo DG, et al. Haploinsufficiency of nadph oxidase subunit neutrophil cytosolic factor 2 is sufficient to accelerate full-blown lupus in nzm 2328 mice. *Arthritis Rheumatol*. 2017;69(8): 1647-1660.
27. Rojas Márquez JD, Li T, McCluggage ARR, et al. Cutting edge: NOX2 NADPH oxidase controls infection by an intracellular bacterial pathogen through limiting the type 1 IFN response. *J Immunol*. 2021; 206(2):323-328.
28. Song Z, Huang G, Chiquetto Paracatu L, et al. NADPH oxidase controls pulmonary neutrophil infiltration in the response to fungal cell walls by limiting LTB4. *Blood*. 2020;135(12):891-903.
29. Whitmore LC, Hilkin BM, Goss KL, et al. NOX2 protects against prolonged inflammation, lung injury, and mortality following systemic insults. *J Innate Immun*. 2013;5(6):565-580.
30. Whitmore LC, Goss KL, Newell EA, Hilkin BM, Hook JS, Moreland JG. NOX2 protects against progressive lung injury and multiple organ dysfunction syndrome. *Am J Physiol Lung Cell Mol Physiol*. 2014;307(1):L71-L82.
31. Bagaitkar J, Pech NK, Ivanov S, et al. NADPH oxidase controls neutrophilic response to sterile inflammation in mice by regulating the IL-1α/G-CSF axis. *Blood*. 2015;126(25):2724-2733.
32. Misharin AV, Morales-Nebreda L, Mutlu GM, Budinger GR, Perlman H. Flow cytometric analysis of macrophages and dendritic cell subsets in the mouse lung. *Am J Respir Cell Mol Biol*. 2013;49(4):503-510.
33. Liu Z, Gu Y, Chakarov S, et al. Fate mapping via Ms4a3-expression history traces monocyte-derived cells. *Cell*. 2019;178(6): 1509-1525.e1519.
34. Kamei A, Gao G, Neale G, et al. Exogenous remodeling of lung resident macrophages protects against infectious consequences of bone marrow-suppressive chemotherapy. *Proc Natl Acad Sci USA*. 2016;113(41): E6153-E6161.
35. Duan M, Li WC, Vlahos R, Maxwell MJ, Anderson GP, Hibbs ML. Distinct macrophage subpopulations characterize acute infection and chronic inflammatory lung disease. *J Immunol*. 2012;189(2): 946-955.
36. Yin C, Cheng L, Pan J, et al. Regulatory role of Gpr84 in the switch of alveolar macrophages from $CD11b^{lo}$ to $CD11b^{hi}$ status during lung injury process. *Mucosal Immunol*. 2020;13(6):892-907.
37. Machiels B, Dourcy M, Xiao X, et al. A gammaherpesvirus provides protection against allergic asthma by inducing the replacement of resident alveolar macrophages with regulatory monocytes [published correction appears in *Nat Immunol*. 2018;19(9):1035]. *Nat Immunol*. 2017;18(12):1310-1320.
38. Guo L, Johnson RS, Schuh JC. Biochemical characterization of endogenously formed eosinophilic crystals in the lungs of mice. *J Biol Chem*. 2000;275(11):8032-8037.
39. Hoenerhoff MJ, Starost MF, Ward JM. Eosinophilic crystalline pneumonia as a major cause of death in 129S4/SvJae mice. *Vet Pathol*. 2006;43(5):682-688.
40. Clausen BE, Burkhardt C, Reith W, Renkawitz R, Förster I. Conditional gene targeting in macrophages and granulocytes using LysMcre mice. *Transgenic Res*. 1999;8(4): 265-277.
41. Liberzon A, Birger C, Thorvaldsdóttir H, Ghandi M, Mesirov JP, Tamayo P. The Molecular Signatures Database (MSigDB) hallmark gene set collection. *Cell Syst*. 2015; 1(6):417-425.
42. Fujioka S, Niu J, Schmidt C, et al. NF-kappaB and AP-1 connection: mechanism of NF-kappaB-dependent regulation of AP-1 activity. *Mol Cell Biol*. 2004;24(17): 7806-7819.
43. Kelkka T, Kienhöfer D, Hoffmann M, et al. Reactive oxygen species deficiency induces autoimmunity with type 1 interferon signature. *Antioxid Redox Signal*. 2014; 21(16):2231-2245.
44. Frevert CW, Felgenhauer J, Wygrecka M, Nastase MV, Schaefer L. Danger-associated molecular patterns derived from the extracellular matrix provide temporal control

of innate immunity. *J Histochem Cytochem*. 2018;66(4):213-227.

45. Erridge C. Endogenous ligands of TLR2 and TLR4: agonists or assistants? *J Leukoc Biol*. 2010;87(6):989-999.

46. Ley K, Pramod AB, Croft M, Ravichandran KS, Ting JP. How mouse macrophages sense what is going on. *Front Immunol*. 2016;7:204.

47. Segal BH, Han W, Bushey JJ, et al. NADPH oxidase limits innate immune responses in the lungs in mice. *PLoS One*. 2010;5(3):e9631.

48. Morgenstern DE, Gifford MA, Li LL, Doerschuk CM, Dinauer MC. Absence of respiratory burst in X-linked chronic granulomatous disease mice leads to abnormalities in both host defense and inflammatory response to Aspergillus fumigatus. *J Exp Med*. 1997;185(2):207-218.

49. Volman TJ, Hendriks T, Goris RJ. Zymosan-induced generalized inflammation: experimental studies into mechanisms leading to multiple organ dysfunction syndrome. *Shock*. 2005;23(4):291-297.

50. Potera RM, Cao M, Jordan LF, Hogg RT, Hook JS, Moreland JG. Alveolar macrophage chemokine secretion mediates neutrophilic lung injury in Nox2-deficient mice. *Inflammation*. 2019;42(1):185-198.

51. Han W, Li H, Cai J, et al. NADPH oxidase limits lipopolysaccharide-induced lung inflammation and injury in mice through reduction-oxidation regulation of NF-κB activity. *J Immunol*. 2013;190(9):4786-4794.

52. Dumas A, Knaus UG. Raising the 'good' oxidants for immune protection. *Front Immunol*. 2021;12:698042.

53. Bekkering S, Domínguez-Andrés J, Joosten LAB, Riksen NP, Netea MG. Trained immunity: reprogramming innate immunity in health and disease. *Annu Rev Immunol*. 2021;39(1):667-693.

54. Kulikauskaite J, Wack A. Teaching old dogs new tricks? The plasticity of lung alveolar macrophage subsets. *Trends Immunol*. 2020;41(10):864-877.

55. Aegerter H, Kulikauskaite J, Crotta S, et al. Influenza-induced monocyte-derived alveolar macrophages confer prolonged antibacterial protection. *Nat Immunol*. 2020;21(2):145-157.

56. Roquilly A, Jacqueline C, Davieau M, et al. Alveolar macrophages are epigenetically altered after inflammation, leading to long-term lung immunoparalysis [published correction appears in *Nat Immunol*. 2020;21(8):962]. *Nat Immunol*. 2020;21(6):636-648.

57. Yao Y, Jeyanathan M, Haddadi S, et al. Induction of autonomous memory alveolar macrophages requires T cell help and is critical to trained immunity. *Cell*. 2018;175(6):1634-1650.e1617.

58. Lavin Y, Mortha A, Rahman A, Merad M. Regulation of macrophage development and function in peripheral tissues. *Nat Rev Immunol*. 2015;15(12):731-744.